ELSEVIER

Physica B 318 (2002) 97–105

PHYSICA B

www.elsevier.com/locate/physb

Chemical physics of metallic clathrates with low carrier concentration ☆

F. Steglich*, A. Bentien, M. Baenitz, W. Carrillo-Cabrera, F.M. Grosche[1], C. Langhammer, S. Paschen, G. Sparn, V.H. Tran, H.Q. Yuan, Yu. Grin

Max-Planck Institute for Chemical Physics of Solids, 01187 Dresden, Germany

Abstract

We discuss physical properties of two metallic clathrate compounds with low carrier concentration: $Eu_8Ga_{16}Ge_{30}$, the first clathrate known to date, for which the 'guest' sites are fully occupied by 'rattling' lanthanide ions, and Ba_6Ge_{25}. $Eu_8Ga_{16}Ge_{30}$ exists in two modifications which both contain divalent Eu ions and order ferromagnetically at low temperatures ($T_C = 10.5$ K and 36 K, respectively). In Ba_6Ge_{25} some of the 'rattling' Ba atoms lock, perhaps randomly, into split positions near 200 K. A BCS-like superconducting phase transition takes place at $T_c = 0.14$ K. T_c increases almost 20-fold, as the structural distortion is suppressed under hydrostatic pressure.

Keywords: Clathrates; Bad metal; Ba_6Ge_{25}; $Eu_8Ga_{16}Ge_{30}$; New materials

1. Introduction

Clathrates are cubic solids built up by large cages of silicon, germanium or tin (or even H_2O) which encapsulate 'guest' atoms. The cages are face sharing and their constituent atoms tetrahedrally (sp^3-like) bonded. A large variety of systems has been obtained by partial substitution of cage atoms and/or by introducing different 'guest' atoms into the cages. The bonding situation of clathrates may, in a first approximation, be understood in terms of the common chemical valence (Zintl) concept [1]. In a Zintl compound, each constituent attains a closed valence shell by combining a formal charge transfer with covalent bonds: The more electropositive 'guest' atoms donate electrons to the more electronegative host (or cage) atoms such that the latter complete their valence requirement (octet rule) and establish a covalently bonded cage structure. The 'guest' atoms, on the other hand, are weakly ionically bonded to the host framework. Since in this simple concept all valence electrons are used in the covalent bonds, one would expect clathrates to be semiconductors. However, the real situation is more complex, and semiconducting clathrates appear to be rather an exception than the rule.

The renewed interest in clathrates [2–4] derives from the claim that they behave as 'phonon glasses' and 'electron crystals' and, therefore, are promising thermoelectric materials. Atoms

☆ Dedicated to Professor Zachary Fisk on the occasion of his 60th birthday.

*Corresponding author. Tel.: +49-351-46-463900; fax: +49-351-46-463902.

E-mail address: steglich@cpfs.mpg.de (F. Steglich).

[1] Present address: Royal Holloway, University of London, Egham, Surrey TW20 OEX, UK.

0921-4526/02/$ - see front matter
PII: S0921-4526(02)00781-0

encapsulated in oversized atomic cages are believed to undergo large local anharmonic vibrations, somewhat independent of the other atoms in the crystal. These 'Einstein modes' may resonantly scatter the heat-carrying acoustic Debye phonons, i. e., the 'rattling' may lead to very low and 'glassy' thermal conductivities κ ('phonon glasses'), provided that $\kappa(T)$ is phonon dominated. On the other hand, the residual electronic charge carriers are propagating along the host framework and are, therefore, much less affected by the 'rattling' than the Debye phonons. Compared to $\kappa(T)$, the electrical conductivity $\sigma(T)$ is relatively larger, which results in an enhanced thermoelectric figure of merit, $Z = S^2\sigma/\kappa$, where S denotes the thermoelectric power.

The joint effort concerning clathrates by chemists and physicists at the MPI-CPfS is aimed at finding small-gap semiconductors/semimetals ('Kondo Insulators', KI) [5], i.e., by substituting suitable lanthanides with an unstable 4f shell for the 'guest' atoms in such cases where they are divalent alkaline-earth atoms, e.g., Sr or Ba. Since KI exhibit giant $S(T)$ values (see e.g. [6]), the dimensionless thermoelectric figure of merit, ZT, may become sufficiently large at low temperatures, such that clathrate-based KI might eventually be used for cryogenic Peltier refrigeration. Apart from these promising thermoelectric properties, these materials offer the study of strongly correlated, low-density charge-carrier systems in a new chemical environment, quite different from that in most KI known so far [5].

In the first part of this paper, we address $Eu_8Ga_{16}Ge_{30}$, the only clathrate known to date in which 100% of the 'guest' sites are occupied by lanthanide ions. While this material has been shown [7–10] to exist in its so-called β-modification, we have recently found [11] that there exists another modification, α-$Eu_8Ga_{16}Ge_{30}$. The latter is the thermodynamically stable one at low temperatures. Both modifications contain a periodic lattice of Eu^{2+} ions. They are ferromagnetically ordered metals with small carrier concentration and low Curie temperatures (10.5 and 36 K, respectively). Currently, efforts are being made in our institute to modify the Ga–Ge framework in order to suppress magnetic order and establish a KI state.

The second part of the paper is devoted to Ba_6Ge_{25}, which may be considered a reference compound for a potential KI. This compound has been discovered in our institute [12], and its existence was recently confirmed by two other groups [13,14]. Two of its three inequivalent Ba sites being occupied by 'rattling' atoms, Ba_6Ge_{25} shows a striking deviation from the concept of 'electron crystals'. This concept is based upon the assumption that the lattice degrees of freedom related to the 'rattling' are essentially decoupled from the electronic degrees of freedom. However, a reduction of the 'rattling' due to the locking in of some of the Ba atoms, accompanied by two closely spaced first-order structural phase transitions at $T_{s1} = 215\,\mathrm{K}$ and $T_{s2} = 180\,\mathrm{K}$, causes a strong reduction of the charge-carrier mobility. This mobility reduction could be caused by an increase of the scattering rate due to disorder created by a *random* locking of the Ba atoms and/or by an increase of the effective mass of the charge carriers via the formation of polaronic quasiparticles [15]. Here, we take the former point of view adopted in Ref. [16] and consider Ba_6Ge_{25} to behave, below $T = T_{s2}$, as a 'bad metal'. The latter undergoes a superconducting phase transition at $T_c \sim 0.14\,\mathrm{K}$. Under hydrostatic pressure, $p_c = 2.8\,\mathrm{GPa}$, the structural transitions are suppressed, whereas T_c increases by almost a factor of 20. This observation hints at a pressure-induced decrease of the disorder caused by the random displacement of Ba atoms below T_{s2}.

2. The ferromagnet $Eu_8Ga_{16}Ge_{30}$

In its new α-phase, $Eu_8Ga_{16}Ge_{30}$ is stable below 696°C, while the β-phase exists as the stable modification at higher temperatures. For the structure refinement of single crystals and the preparation of single-phase polycrystalline ingots of both modifications, we refer to Ref. [11]. Fig. 1 displays the crystal structures of the two modifications. These are, in both cases, characterized by covalent E_{46} (E = Ga, Ge) networks of fourfold bonded (4b) E atoms with polyhedral cages occupied by Eu atoms. The β-phase has two kinds of polyhedral cages: E_{20} pentagonal dodecahedra

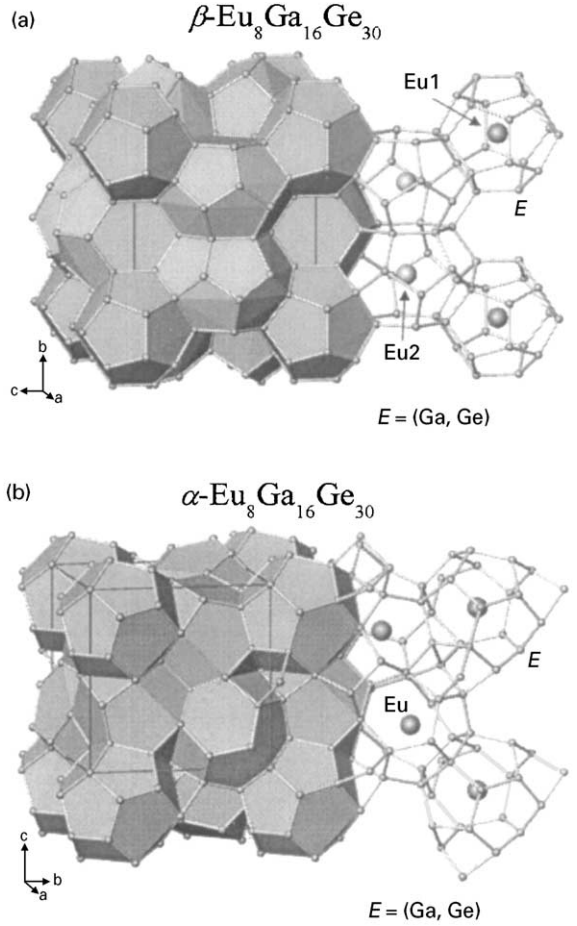

Fig. 1. Crystal structures of β- and α-$Eu_8Ga_{16}Ge_{30}$.

centered by Eu1 and E_{24} tetrakaidecahedra centered by Eu2. There are two Eu1 and six Eu2 atoms per $Eu_8Ga_{16}Ge_{30}$ formula unit. Characteristic for the β-phase is the non-intersecting threefold rod packing formed by the Eu2 sites along the $\langle 1\,0\,0 \rangle$ directions. The α-phase has only one type of cage centered by Eu. This cage can be described as a distorted E_{20+3} polyhedron, derived from an E_{20} pentagonal dodecahedron via breaking three E–E bonds and creating nine new ones by adding three more E atoms. The edge of the central Eu_4 tetrahedron has a length of 5.590 Å. The Eu1 and Eu2 atoms in the β-phase as well as the Eu atoms in the α-phase are 'rattling', according to single-crystal X-ray diffraction-intensity data [11].

Since Ga and Ge cannot be distinguished by X-rays, it was assumed in the structure refinement that the Ga and Ge atoms are distributed at random among the E sites. However, a short E2–E2 bond (2.449 Å) in the β-phase suggests a preferential occupation of the E2 sites by Ge atoms. All other E–E bond lengths are between 2.471 and 2.503 Å, consistent with a random distribution of the Ga and Ge atoms. The smallest Eu–Eu distance in α-$Eu_8Ga_{16}Ge_{30}$ is 5.562 Å. In β-$Eu_8Ga_{16}Ge_{30}$ it is distinctively shorter: 5.23 Å. The average distance between Eu and E-atoms of the surrounding cage is 3.633 Å for α-$Eu_8Ga_{16}Ge_{30}$, while for β-$Eu_8Ga_{16}Ge_{30}$ the average Eu1–E and Eu2-E distances are 3.482 and 3.846 Å, respectively.

Applying the Zintl concept [1] to $Eu_8Ga_{16}Ge_{30}$, one expects the two valence electrons of Eu^{2+} on all Eu sites to be transferred to the E cages such that the sp^3-like bonds between the Ga/Ge atoms can be formed for both modifications. However, rather than behaving as semiconductors, both the β- and the α-phase show a positive temperature coefficient of the electrical resistivity $\rho(T)$, except for a narrow temperature window above the respective Curie temperatures, where critical fluctuations may come into play [11].

In addition, for both modifications the Hall resistivity, $\rho_H(B)$, is a linear function of the magnetic field in the paramagnetic regime, above the Curie temperatures. Therefore, the Hall data may be analyzed by assuming only one type of charge carriers (i.e., electrons) to be present. Such an analysis yields carrier densities of $1\text{–}1.5 \times 10^{21}\,\mathrm{cm}^{-3}$ for the α-phase and $\approx 0.5 \times 10^{21}\,\mathrm{cm}^{-3}$ for the β-phase [11]. These values are rather low when compared to simple metals, but deviate substantially from zero as derived within the Zintl concept. The Hall mobilities were found to be relatively low, i.e., ≈ 50 and $20\,\mathrm{cm}^2/\mathrm{V\,s}$ at low temperature as well as 20 and $7\,\mathrm{cm}^2/\mathrm{V\,s}$ at 300 K for the α- and β-phase, respectively.

Fig. 2 shows the temperature dependence of the magnetic susceptibility, $\chi(T)$ of α- and β-$Eu_8Ga_{16}Ge_{30}$, measured in a magnetic field $B = 0.1$ T. At the lowest temperatures, $\chi(T)$ is almost constant but starts to decrease strongly above ≈ 8 and 20 K for the α- and β-phase sample,

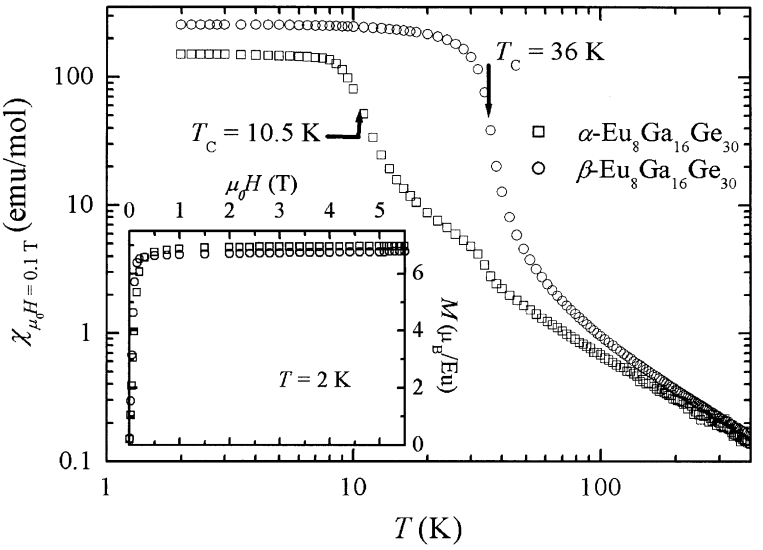

Fig. 2. Magnetic susceptibility, χ, for α- and β-$Eu_8Ga_{16}Ge_{30}$, measured in a magnetic field of 0.1 T, as a function of temperature, T. Inset shows magnetization, $M(H)$, curves at $T = 2$ K.

respectively. Upon cooling the samples in zero magnetic field (not shown), a spontaneous magnetization M builds up for the two samples, pointing to ferromagnetic phase transitions with Curie temperatures, T_C, of 10.5 and 36 K. Well above T_C, $\chi(T)$ exhibits Curie–Weiss-type temperature dependences with effective magnetic moments of 7.8 and 7.9 μ_B per Eu ion and Weiss temperatures of 11 and 34 K for the α- and β-phase sample, respectively. The moments are in good agreement with the effective moment of 7.9 μ_B expected for a free Eu^{2+} ion and the Weiss temperatures are close to the Curie temperatures. The field dependences of the magnetization at 2 K (inset of Fig. 2) are typical of soft ferromagnets: $M(B)$ first increases steeply with the field and then saturates at a constant value. Within the experimental resolution ($\approx$10 Oe) of our magnetometer, no hysteresis could be resolved. The saturation magnetization of 7 μ_B expected for a free Eu^{2+} ion is almost reached for both samples at 2 K and 5.5 T. Thus, both α- and β-$Eu_8Ga_{16}Ge_{30}$ may be classified as local-moment ferromagnets with Eu being in its Eu^{2+} state in the entire temperature range.

Because of the large Eu–Eu distances, direct exchange between the Eu-4f magnetic moments can be safely discarded. The ferromagnetic coupling between them must be due to the indirect (RKKY) interaction via the oscillatory conduction-electron spin polarization which depends on the charge-carrier concentration. Taking the values of the latter at T_C determined from the Hall coefficients [11], this interaction must be ferromagnetic at Eu–Eu distances smaller than 10 Å (6.5 Å) for α- (β-)$Eu_8Ga_{16}Ge_{30}$. In fact, the nearest neighbor Eu–Eu distances are 5.562 Å (5.23 Å) for α- (β-)$Eu_8Ga_{16}Ge_{30}$. For these distances, the absolute value of the exchange energy is larger for the β- than for the α-modification, in accord with the higher T_C of the former.

The temperature dependences of the specific heat, $C_p(T)$, of α- and β-$Eu_8Ga_{16}Ge_{30}$ are shown in Fig. 3. Pronounced λ-type anomalies are observed in the temperature ranges of the ferromagnetic phase transitions discussed above. As is explained in detail in Ref. [11], three contributions to the total specific heat could be separated, i.e., the lattice contribution $C_L(T)$, the electronic contribution $C_e(T)$, and the magnetic contribution $C_m(T)$. The lattice contribution was taken from the non-magnetic reference compound $Ba_8Ga_{16}Ge_{30}$. $C_p(T)$ of $Ba_8Ga_{16}Ge_{30}$ is also shown in Fig. 3. A good description of the latter data is achieved with $C_p(T) = C_L(T) + C_e(T)$, where the

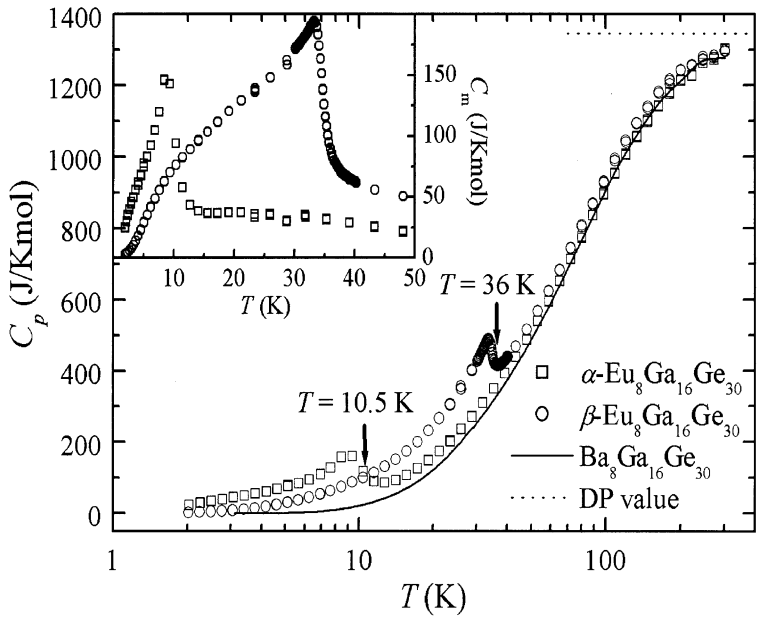

Fig. 3. Temperature dependence of the specific heat, $C_p(T)$, for α- and β-$Eu_8Ga_{16}Ge_{30}$ as well as for $Ba_8Ga_{16}Ge_{30}$. Dulong–Petit value is also indicated. The magnetic contributions, $C_m(T)$, obtained as explained in the text, are shown in the inset.

electronic term is calculated from the Hall coefficient, assuming that the effective mass of the charge carriers is equal to the free-electron mass. The lattice contribution was described by the sum of a Debye and an Einstein term [11].

The magnetic contributions to the total $C_p(T)$ of α- and β-$Eu_8Ga_{16}Ge_{30}$ were obtained by subtracting the lattice contribution of $Ba_8Ga_{16}Ge_{30}$ as well as the electronic contributions of the respective modifications, again estimated from the Hall coefficients under the same assumption mentioned above. $C_m(T)$ is shown for both samples in the inset of Fig. 3. The T_C values determined in a plot C_m/T vs. T by replacing, in an entropy-conserving way, the broadened transitions by idealized sharp ones are in good agreement with those obtained from the magnetic measurements. The molar magnetic entropies at T_C amount to 90% and 145% of the theoretical value, $R\ln(2S+1)$ with $S = 7/2$, proving that the ferromagnetic transitions are bulk effects in either system. The relatively poor agreement with the theoretical entropy value has been ascribed to the fact that $Ba_8Ga_{16}Ge_{30}$ is not a perfect reference system for its Eu homologue [11].

In summary, both the α- and β-phase of $Eu_8Ga_{16}Ge_{30}$ are local-moment ferromagnets with low Curie temperatures. Due to the positive T-coefficient of the electrical resistivity the two systems behave metallic, though exhibiting small charge-carrier concentrations as, in fact, expected from the charge-balanced Zintl count. The Hall mobilities have been found to be relatively small. This is due to substantial disorder on the Ga–Ge framework and/or to a non-negligible interaction between the charge carriers and the 'rattle' modes of the Eu^{2+} ions. Obviously, the latter possibility would question the validity of the concept of an 'electron crystal' [2–4] for $Eu_8Ga_{16}Ge_{30}$. On the other hand, the lattice contribution to the thermal conductivity (Ref. [11]) yields evidence for a strong scattering of the heat-carrying acoustic phonons from those 'rattle' modes and, thus, support the concept of a 'phonon glass' [2–4]. Future efforts shall be made, via alternative synthesis procedures and/or slight modifications of $Eu_8Ga_{16}Ge_{30}$ by chemical substitutions, towards a valence change

from the stable Eu^{2+} to an intermediate-valent (IV) $Eu^{(2+\delta)+}$ configuration. This will, hopefully, cause the suppression of ferromagnetic order and the opening of a narrow (pseudo) gap in the large 4f density of states at the Fermi level of $Eu_8Ga_{16}Ge_{30}$, typical of 'Kondo Insulators' [5].

3. Structural and superconducting phase transitions in Ba_6Ge_{25}

Ba_6Ge_{25} belongs to the structure family of chiral clathrates cP124 and is a binary variant of the $Ba_6In_4Ge_{21}$ type [17], cf. Fig. 4. Ba_6Ge_{25} is cubic with the room-temperature lattice constant $a = 14.5564(2)$ Å. Each unit cell contains four Ba_6Ge_{25} formula units. There are three different lattice sites for the Ba atoms in the structure. Each of the Ge_{20} polyhedra is centered by a Ba atom (Ba1 site) and the two remaining Ba atoms occupy cavities in the zeolite-like labyrinth created by the non-space-filling three-dimensional arrangement of the Ge_{20} polyhedra (Ba2 and Ba3 sites). There

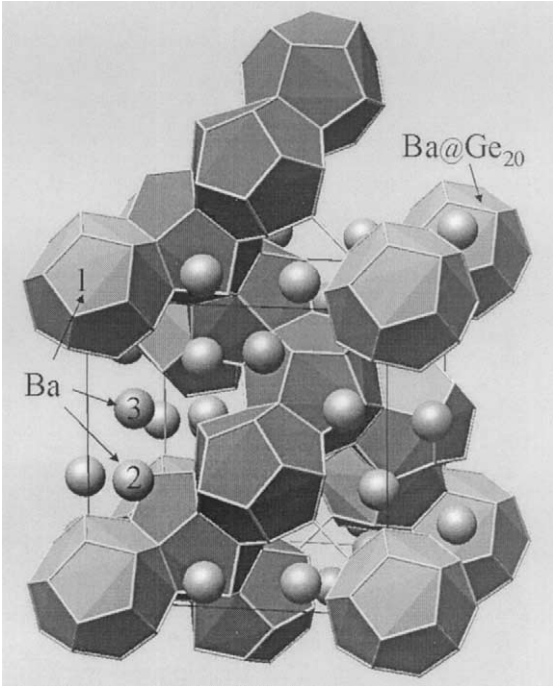

Fig. 4. Crystal structure of Ba_6Ge_{25}.

are two Ba1 sites, three Ba2 sites and one Ba3 site per Ba_6Ge_{25} formula unit. The structure requires the existence of both threefold-bonded (3b) and fourfold-bonded (4b) Ge atoms. In terms of the Zintl concept [1], Ba_6Ge_{25} may be written as $(Ba^{2+})_6((3b)Ge^{1-})_8((4b)Ge^0)_{17}(4e^-)$ [12,18]. Thus, four conduction electrons are expected per Ba_6Ge_{25} unit, corresponding to a relatively small charge-carrier concentration of $\approx 5 \times 10^{21}\,\mathrm{cm}^{-3}$. In the following, a short survey is given on the physical properties of Ba_6Ge_{25} emphasizing its various phase transitions. For more detailed discussions, we refer to two publications [15,16].

The electrical resistivity, $\rho(T)$, of Ba_6Ge_{25} displays a two-step anomaly at ambient pressure at $T_{s1} \approx 215\,\mathrm{K}$ and $T_{s2} \approx 180\,\mathrm{K}$ (on cooling), with strong thermal hysteresis indicating two closely spaced first-order transitions (Fig. 5). Above T_{s1}, the system exhibits metallic behavior, whereas the resistivity undergoes a drastic increase through the transition at T_{s2} to about $1\,\mathrm{m\Omega\,cm}$. Below this jump, the resistivity continues to rise and saturates below 10 K at about $\rho_0 = 1.5\,\mathrm{m\Omega\,cm}$ (inset (a) of Fig. 5). Strikingly, below a further sharp increase in $\rho(T)$ a superconducting transition occurs, with the mid-point of the resistivity jump at $T_c \approx 0.24\,\mathrm{K}$. By applying hydrostatic pressure, the structural transition is depressed to lower temperature and the residual resistivity ρ_0 is reduced, whereas T_c increases drastically. At the critical pressure $p_c = 2.8\,\mathrm{GPa}$, where the structural distortion is suppressed completely, the resistively determined T_c reaches a maximum of 3.85 K and a metallic resistivity appears, if with a large residual value, over the entire temperature range (main part of Fig. 5).

The resistive upper-critical-field curve, $B_{c2}(T)$, has been determined with $B_{c2}(0) \simeq 0.6\,\mathrm{T}$, and an initial slope of $\mathrm{d}B_{c2}/\mathrm{d}T \simeq -2.9\,\mathrm{T/K}$, corresponding to a coherence length of about 280 Å. This value is consistent with a 'dirty-limit' conventional (BSC) superconductor [16]: $\mathrm{d}B_{c2}/\mathrm{d}T = -(12e/\pi^3 k_B)\gamma\rho_0 V_m^{-1} \simeq -3\,\mathrm{T/K}$, where $\gamma = C_e/T$ is the Sommerfeld coefficient of the normal-state electronic specific heat (see Fig. 6) and V_m refers to the molar volume. The electronic mean free path can be estimated by standard methods, e.g. [16], as

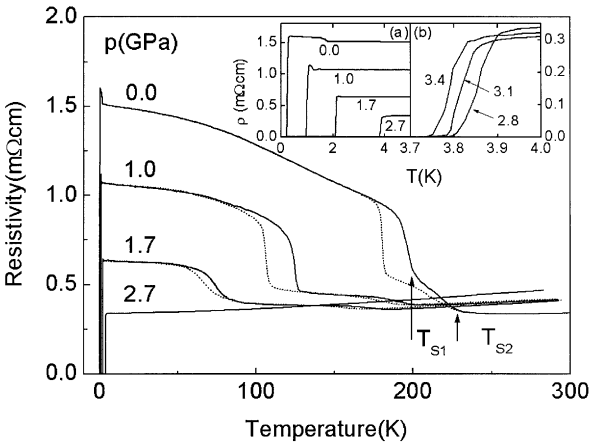

Fig. 5. Temperature dependence of the resistivity, $\rho(T)$, of Ba_6Ge_{25} at different hydrostatic pressures. Solid and dashed lines describe warming-up and cooling-down processes, respectively. A two-step structural transition occurs at T_{s1} and T_{s2}, indicated by the arrows. Insets show the transitions to superconductivity in detail: (a) T_c is strongly enhanced when the structural transition is depressed by pressure, (b) pressures above p_c lead to a slight decrease of T_c.

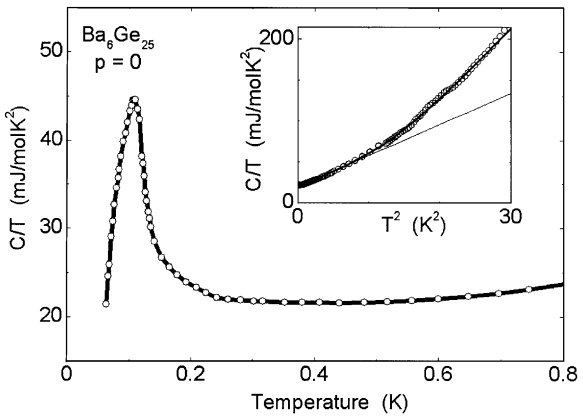

Fig. 6. Specific-heat coefficient C/T vs. T for Ba_6Ge_{25} at low T (main figure) and plotted vs. T^2 up to approx. 5 K (inset). The low-temperature data show a bulk superconducting transition with reduced jump height $\Delta C/\gamma T_c$ of 1.47. Above about 3 K, the specific heat is no longer well approximated by a Debye T^3 law (lower line in inset, obtained by fitting $C/T = \gamma + \beta T^2$ to the low-temperature data, with $\beta = 3.8\,\mathrm{mJ/molK^4}$ ($\theta_D \simeq 250\,\mathrm{K}$) and $\gamma \simeq 21\,\mathrm{mJ/mol\,K^2}$). A single additional Einstein mode at energy $\hbar\Omega/k_B = 37.2\,\mathrm{K}$ is sufficient to obtain satisfactory agreement (upper line in the inset).

$\ell \simeq 1200\,\text{Å} \times (A_F/(4\pi\,\text{Å}^2)\rho_0/\mu\,\Omega\,\mathrm{cm})^{-1}$. Here, A_F refers to the total Fermi surface area and would be minimized for a single spherical Fermi surface, where this expression gives $\ell \approx 3\,\text{Å}$ in Ba_6Ge_{25}, justifying the use of the above 'dirty-limit' expression.

Bulk superconductivity in Ba_6Ge_{25} is inferred from measurements of the specific heat (Fig. 6). The specific-heat results reveal a normal-state metallic C_e/T-ratio of $\gamma \simeq 21\,\mathrm{mJ/molK^2}$ above a broadened transition with an onset at 0.27 K, consistent with the onset of the resistive transition, and a bulk transition temperature of about 0.14 K, in agreement with susceptibility data (not shown). The ratio of the jump height to $C_e(T_c)$, estimated by applying an entropy-conserving ('equal-areas') construction, is about 1.47, close to the BCS value of 1.43. The discrepancy between the resistive and bulk T_c is attributed to inhomogeneities, resulting in a distribution of T_c across the sample if the transition temperature depends strongly on the precise sample composition.

At higher temperatures, one observes only a small region in which a Debye-like temperature dependence of the specific heat is obeyed (inset of Fig. 6). Above about 2 K, the specific heat increases more rapidly, indicating a significant contribution of low-lying localized (Einstein) modes. The specific heat is consistent with the contribution expected from a single Einstein mode per formula unit at energy $\hbar\Omega \simeq k_B \times 37.2\,\mathrm{K}$. As only the Ba3 position is unique, while there are

several Ba1 and Ba2 positions per formula unit, the lowest Einstein mode is ascribed to the 'rattling' of the Ba3 atom. The latter assumes an off-symmetry, split position at low temperatures [19] which is accompanied by a narrowing of the potential well, leading to an increased frequency of oscillation.

In Refs. [15,16], several physical properties are compared between Ba_6Ge_{25} and its Na-derivative in which two of the three Ba2 sites are randomly occupied by Na. Most strikingly, the reference compound $Ba_4Na_2Ge_{25}$ is lacking the structural phase transitions. It shows a 50% higher Sommerfeld coefficient, despite its lower nominal carrier concentration, and a T_c of 0.83 K, which is six times greater than that of Ba_6Ge_{25}. It was argued [16] that the enormous difference in T_c between the two systems must be related to differences in the electron–phonon coupling constant λ, rather than in the spectrum of the Debye phonons. In this reasoning, λ appears to be driven by two effects: an increase of the bare (bandstructure) electronic density of states and a softening of the Einstein mode associated with the Ba3 atom on going from Ba_6Ge_{25} to $Ba_4Na_2Ge_{25}$. Both effects were traced back to the fact [16] that the large random displacements of Ba atoms on sites 2 and 3, found by X-ray diffraction studies at the structural transitions in Ba_6Ge_{25}, are lacking for $Ba_4Na_2Ge_{25}$. In the former compound, the resulting disorder then leads to a strong random scattering and, thus, a strong reduction of the charge-carrier mobility [15]. Since $k_F\ell \approx 1$ (k_F being the Fermi wave number and $\ell \approx 3$ Å), structurally disordered Ba_6Ge_{25} is close to the 'bad-metal' limit. In the most straightforward interpretation, the high level of disorder effectively smears out, via collision-time broadening, any structure in reciprocal space on a scale finer than $1/\ell$ and hence smoothes the density of states over $\delta E \simeq \hbar v_F/\ell$, where v_F refers to the Fermi velocity. In the present case, where E_F lies close to the band edge a significant reduction of the density of states can result, if $\hbar v_F/\ell > E_F$, which is automatically satisfied in the 'bad-metal' limit. Other mechanisms may contribute further to a reduction of the density of states on entering the distorted low-T state. For instance, detailed X-ray studies suggest [19] that at $T_{s1,s2}$ there is a tendency for some of the Ba atoms to dimerize: atoms on sites 2 and 3 approach each other, giving rise to a static, ferroelectric distortion inside the unit cell. Preliminary bandstructure calculations [20] indicate that the resulting crystalline potential rearranges the conduction bands, enhancing the electron density in the attractive region between the two displaced Ba atoms and further reducing the electronic density of states at E_F. In a more local picture, this may be seen to correspond to the formation of a Ba–Ba bond, dynamically occupied by electrons contributing to the Fermi sea [15].

The main conclusion drawn from the comparison between Ba_6Ge_{25} and its Na-derived homologue, i.e., the enormous enhancement of the superconducting transition temperature freeing the Ba atoms from their split positions on going from the former to the latter compound, can be confirmed by applying hydrostatic pressure to Ba_6Ge_{25}. As illustrated in Fig. 7, this furnishes a decrease of the structural transition temperatures T_{s1} and T_{s2} and, simultaneously, an increase in T_c. At $p_c = 2.8$ GPa, where the structural instability is suppressed to $T = 0$, T_c has increased almost 20-fold. This suggests that, as Ba_6Ge_{25} approaches

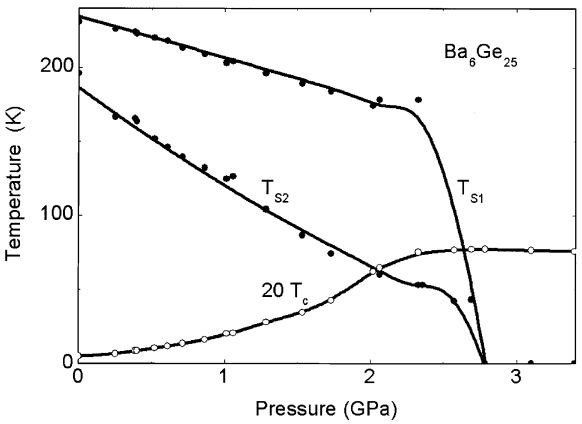

Fig. 7. Pressure-temperature phase diagram of Ba_6Ge_{25}. The resistivity anomalies observed on warming at $T_{s1,s2}$ (closed symbols, onset temperature for T_{S1}, mid-point of jump for T_{s2}) are associated with the lock-in transitions of Ba2 and Ba3 atoms. They are suppressed rapidly with increasing hydrostatic pressure, along with a dramatic increase of the superconducting transition temperature, T_c (open symbols, mid-point of the resistivity drop), which reaches 3.85 K at 2.8 GPa.

the undistorted high-pressure structure, the combined effect of an increase in the bare density of states and of a shift of phonon spectral weight to lower energies enhances λ and increases T_c. Both mechanisms can be more effective, if pressure is applied instead of chemical substitution: the ultimate density of states in undistorted Ba_6Ge_{25} is expected to be higher than that of $Ba_4Na_2Ge_{25}$ because of the higher nominal electron count, and the phonon spectrum at p_c can be softer than that of the reference compound, which is at ambient pressure far away from the lattice instability. At $p > p_c$, T_c is found to decrease again (cf. inset (b) of Fig. 5), qualitatively similar to preliminary results for $Ba_4Na_2Ge_{25}$ showing $dT_c/dp < 0$ already at low pressures [21].

4. Conclusion

Filled-cage systems like the clathrate compounds are interesting for future materials research. These studies will benefit from, if not require, a close collaboration between solid-state chemists and physicists. Here, we have reported such efforts focussing on the only clathrate known so far, for which the 'guest' sites are fully occupied by lanthanide ions, $Eu_8Ga_{16}Ge_{30}$, as well as on the binary compound Ba_6Ge_{25}. In order to transform these compounds into new strongly correlated semiconductors/semimetals, an IV state of Eu has to be achieved by chemical means in the former compound, while Ba^{2+} has to be replaced by a suited IV lanthanide ion in the latter one.

Acknowledgements

We are grateful to H. Borrmann and R. Cardoso Gil for the single-crystal X-ray diffraction and R. Niewa for the DTA measurements. Useful discussions with P. Thalmeier, I. Zerec and F. Kromer are also acknowledged. Part of this work was supported by the Fonds der Chemischen Industrie.

References

[1] H. Schäfer, Ann. Rev. Mater. Sci 15 (1985) 1.
[2] G.S. Nolas, et al., Appl. Phys. Lett. 73 (1998) 178.
[3] N.P. Blake, et al., J. Chem. Phys. 111 (1999) 3133.
[4] G.A. Slack, in: D.M. Rowe (Ed.), CRC Handbook of Thermoelectrics, Chemical Rubber, Boca Raton, FL, 1995 (Chapter 34).
[5] G. Aeppli, Z. Fisk, Comments Cond. Mater. Phys. 16 (1992) 155 and references cited therein.
[6] S. Paschen, et al., Phys. Rev. B. 62 (2000) 14912.
[7] J.L. Cohn, et al., Phys. Rev. Lett. 82 (1999) 779.
[8] G.S. Nolas, et al., Mater. Res. Soc. Symp. Proc. 545 (1999) 435.
[9] B.C. Sales, et al., Phys. Rev. B 63 (2002) 245113.
[10] B.C. Chakoumakos, et al., J. Alloys Compounds 322 (2001) 12.
[11] S. Paschen, W. Carrillo-Cabrera, A. Bentien, V.H. Tran, M. Baenitz, Yu. Grin, F. Steglich, Phys. Rev. B 64 (2001) 214404.
[12] W. Carrillo-Cabrera, et al., VIIth European Conference on Solid State Chemistry, Madrid, Abstract P24, 1999.
[13] H. Fukuoka, et al., J. Solid State Chem. 151 (2000) 151.
[14] S.-J. Kim, et al., J. Solid State Chem. 153 (2000) 321.
[15] S. Paschen, V.H. Tran, M. Baenitz, W. Carrillo-Cabrera, Yu. Grin, F. Steglich, Phys. Rev. B 65 (2002) 134435.
[16] F.M. Grosche, H.Q. Yuan, W. Carrillo-Cabrera, S. Paschen, C. Langhammer, F. Kromer, G. Sparn, M. Baenitz, Yu. Grin, F. Steglich, Phys. Rev. Lett. 87 (2001) 2470031.
[17] H.G. von Schnering, et al., Z. Kristallogr. NCS 213 (1998) 665.
[18] W. Carrillo-Cabrera, et al., Z. Kristallogr. NCS 215 (2000) 207.
[19] W. Carrillo-Cabrera, Yu. Grin, et al., to be published.
[20] I. Zerec, A. Yaresko, P. Thalmeier, cond-mat/0202318.
[21] H.Q. Yuan, F.M. Grosche, G. Sparn (unpublished results).